# Flower Constellation of Millimeter-Wave Radiometers for Tropospheric Monitoring at Pseudogeostationary Scale

Frank Silvio Marzano, *Senior Member, IEEE*, Domenico Cimini, *Member, IEEE*, Adelaide Memmo, Mario Montopoli, Tommaso Rossi, Mauro De Sanctis, Marco Lucente, Daniele Mortari, *Member, IEEE*, and Sabatino Di Michele

***Abstract*—In this paper, the design of a minisatellite FLOwer constellation (FC), deploying millimeter-wave (MMW) scanning RADiometers, namely, FLORAD, and devoted to tropospheric observations, is analyzed and discussed. The FLORAD mission is aimed at the retrieval of thermal and hydrological properties of the troposphere, specifically temperature profile, water-vapor profile, cloud liquid content, and rainfall and snowfall rate. The goal of frequent revisit time at regional scale, coupled with quasi-global coverage and relatively high spatial resolution, is here called pseudogeostationary scale and implemented through a FC of three minisatellites in elliptical orbits. FCs are built on compatible (resonant) orbits and can offer several degrees of freedom in their design. The payload MMW channels for tropospheric retrieval were selected following the ranking based on a reduced-entropy method between 90 and 230 GHz. Various configurations of the MMW radiometer multiband channels are investigated, pointing out the tradeoff between performances and complexity within the constraint of minisatellite platform. Statistical inversion schemes are employed to quantify the overall accuracy of the selected MMW radiometer configurations.**

***Index Terms*—Atmospheric retrieval, microwave and millimeter-wave radiometry, regional scale, satellite constellations.**

## I. Introduction

MILLIMETER-WAVE (MMW) observation of the atmosphere is becoming an appealing goal within satellite-radiometry applications [1]–[5]. The major technological advantage of MMW radiometers, i.e., system with operating frequency between 30 and 300 GHz (or wavelength between 1 cm and 1 mm), is the reduced size of the overall system, for given performances, with respect to lower frequency microwave (MW) sensors [6]. In addition, MMW sounding can exploit window frequencies and various gaseous absorption bands at 50/60, 118, and 183 GHz [6]–[9]. These bands can be used to estimate tropospheric temperature profiles, water vapor and cloud liquid contents, and to some extent, rainfall and snowfall. The application of MMW spaceborne radiometry can range from numerical weather prediction (NWP) and data assimilation to climate benchmarking, from hydrometeorology to extreme weather nowcasting and civil protection [10]–[21].

Spaceborne MMW radiometers, aboard low-Earth-orbit (LEO) satellites, can also exhibit relatively small field-of-views (FOVs), on the order of some kilometers [22]. However, the temporal resolution of LEO platform observations remains a major drawback with respect to the geosynchronous-Earth-orbit (GEO) satellites (e.g., [20] and [21]). An overpass every about 12 h for a single LEO platform (conditioned to a sufficiently large swath of the scanning MMW radiometer) is usually not enough to catch the typical temporal-scale variation of atmospheric fields. This feature affects the diurnal sampling of atmospheric properties and cannot be improved by resorting to GEO platforms due to their high orbit altitude and consequent degradation of the MMW-sensor FOVs. Indeed, recent efforts have been exploring this GEO option for MMW atmospheric observation [5].

A way to tackle this impasse on the MMW-sensor temporal resolution is to draw our attention to the deployment of a constellation of satellites and to regional scales [22], [24]. The price to pay to push forward this solution is to keep the overall mission budget, from both an engineering and economic point of views, relatively low, satisfying at the same time the mission scientific objectives [25]. This means the need to design the following features: 1) low-weight minisatellite platform (less than 500 kg); 2) light compact MMW radiometer; 3) launch strategy in order to deploy all platforms with only one launcher; and 4) adaptive retrieval scheme able to exploit available sensor data. Another degree of freedom that a satellite constellation may open, with respect to a single-platform mission, is the design of an optimal space-time coverage for atmospheric-monitoring purposes [26]–[28].

Manuscript received October 11, 2008; revised November 29, 2008. First published May 5, 2009; current version published August 28, 2009. This work was supported by Agenzia Spaziale Italiana.

F. S. Marzano is with the Department of Electronic Engineering, University of Rome "La Sapienza," 00184 Rome, Italy, and also with the Center of Excellence CETEMPS, University of L'Aquila, 67010 L'Aquila, Italy (e-mail: marzano@die.uniroma1.it).

D. Cimini, A. Memmo, and M. Montopoli are with the Center of Excellence CETEMPS, University of L'Aquila, 67010 L'Aquila, Italy (e-mail: nico.cimini@aquila.infn.it).

T. Rossi, M. De Sanctis, and M. Lucente are with the Department of Electronic Engineering, University of Rome "Tor Vergata," 00133 Rome, Italy (e-mail: rossi@david.eln.uniroma2.it).

D. Mortari is with the Department of Aerospace Engineering, Texas A&M University, College Station, TX 77843 USA (e-mail: mortari@aero.tamu.edu).

S. Di Michele is with the European Centre for Medium-Range Weather Forecasts (ECMWF), RG2 9AX Reading, U.K. (e-mail: sabatino.dimichele@ecmwf.int).

Color versions of one or more of the figures in this paper are available online at http://ieeexplore.ieee.org.

Digital Object Identifier 10.1109/TGRS.2008.2012349

In this paper, we will discuss the basic concepts of the FLORAD small mission, aimed at designing a constellation of minisatellite MMW radiometers for atmospheric observations on a *pseudogeostationary scale* [29]. The name FLORAD arises from "FLOwer constellation of MMW RADiometers" and indicates the concept of synergy between Flower-constellation (FC) theory and MMW radiometry. The term *pseudogeostationary scale* will be used in this paper to mean a quasi-global scale with high revisit time at regional scale (in this paper, over the Mediterranean region), as discussed in Section II. The mission objective is the retrieval of thermal and hydrological properties of the troposphere, specifically temperature profiles, integrated water vapor (IWV) and cloud liquid content, and light rainfall and snowfall. To this aim, a recently proposed constellation theory, named FC, will be employed to this purpose as described in Section III. Various configurations of the MMW radiometer multiband channels will also be selected using the reduced-entropy technique. Statistical-estimation algorithms to retrieve the requested atmospheric parameters will be used to evaluate the potential of the various radiometric configurations in terms of retrieval error budget, as illustrated in Section IV. Conclusions will be drawn in Section V with a discussion on FLORAD mission features.

## II. FLORAD Small-Mission Concept

The FLORAD small-mission concept is based on the synergetic cocktail of FC theory, MMW radiometry, and minisatellite engineering, driven by the previously introduced concept of *pseudogeostationary scale*.

FCs are a general class of elliptical orbits which can be optimized in order to maximize the revisit-time interval and maximize the spatial coverage at regional scale, ensuring also a repeating ground-track [27], [28]. The FC concept nicely matches the choice of minisatellites as a baseline configuration, since it easily allows us to achieve relatively small size and weight spaceborne platforms (less than 500 kg) at relatively low cost (essential when deploying several identical spaceborne platforms within a constellation). Moreover, the minisatellite solution clearly addresses the choice of small passive sensors with small size and low weight and power consumption, features which cannot be usually satisfied by active sensors [25]. In this respect, MMW technology is the most compatible with the specifications and constraints of minisatellites.

MMW radiometry of the atmosphere is a quite established application due to its capability to sound through clouds and to detect precipitation (e.g., [2]–[9]). Its capabilities, in terms of atmospheric-profile retrieval, are quite consolidated and can be fruitfully exploited for designing an integrated robust inversion algorithm, using both "opaque" and "transparent" MMW frequencies [8], [31]. Of course, infrared (IR) instruments can retrieve atmospheric profiles with a spatial resolution much higher than MW sensors but only in cloud-free areas [15], [19].

Atmospheric monitoring is a major goal of current and future missions [23]. In this context, MW and MMW radiometry plays a relevant role [22]. Examples of well-known radiometers are the Advanced Microwave Sounding Unit (AMSU) aboard NOAA and MetOp satellites, the Special Sensor Microwave Imager Sounder (SSM/IS) aboard DMSP satellites, the Humidity Sounder Brasil aboard Aqua, and the Microwave Humidity Sounder (MHS) aboard MetOp satellites (e.g., [32] and [33]). Both AMSU and SSM/IS have similar capabilities, but the first is a cross-track scanner with an off-nadir angular excursion between $0^\circ$ and $48.3^\circ$, whereas the second is a conical scanner at about $53^\circ$ off-nadir angle. The impact of MW and MMW radiometer data assimilations into NWP has been shown to reduce the prediction error by more than 50% and 15% in the Southern and Northern Hemispheres, respectively (as estimated, considering the geopotential height forecast skills until three-day range) [10]. This is quite impressive when compared with IR sensors, such as High Resolution Infrared Sounder (HIRS) whose error reduction is less than 5%: This is explained considering that more than 85% of HIRS FOVs cannot be used in NWP due to cloud contamination [15].

It is worth recalling that EUMETSAT, within the Post-European Polar System (Post-EPS) plans after 2020, has recently accomplished a mission-requirement document to rank the most urgent future missions among 21 options [23]. The result of this comparative analysis indicates that, after the high-resolution IR sounding, MW sounding is at the second place before scatterometry, visible-IR imaging, and MW imaging. Moreover, a related output of this Post-EPS plan is the list of observation or user-requirements (i.e., independently from cost and technology issues) for four important applications such as global NWP, regional NWP, nowcasting, and climate monitoring [34], [35].

## III. Design of FLORAD Satellite Constellation

All meteorological satellites so far launched are placed in circular orbits (COs), and most of them are Sun-synchronous (SS) [22]. The exploitation of elliptical orbits has been proposed in past years, particularly in terms of using highly elliptical Molniya orbits for frequent observation of high latitudes by optical and IR sensors [26]. Constant perigee can be maintained by choosing the so-called orbit-critical inclination angles equal to $63.4^\circ$ and $116.6^\circ$. Repeating ground track of Sun-asynchronous satellite orbits can also be of some interest for diurnal cycle sampling, data geolocation, satellite tracking, and climate recording (e.g., [12] and [36]).

The theory of FCs is a new methodology proposed to design satellite constellations. FCs is a natural consequence (and extension to $n$ satellites) of the theory of *compatible* orbits (also called *resonant* or repeating ground track) [27], [28]. An orbit is named compatible with respect to a rotating reference frame if the orbital period is synchronized with the rotation period of the reference frame. Let us consider a reference frame fixed with respect to the Earth, so-called Earth-fixed Earth-centered (ECEF) reference frame. The satellites' relative trajectories in the rotating ECEF reference frame constitute a continuous closed-loop symmetric pattern reminiscent of flower petals [37]. Compatible orbits can be easily built upon the assumption of axial symmetric field force model. This would include all zonal harmonics of Earth's gravitational field. However, compatible orbits are still possible when including the complete Earth gravitational model [27]. The FC theory

explains how to place satellites on the same relative trajectory. In this way, the whole constellation is made of satellites that are running along relative trajectory one after another.

### A. Background on FCs

Compatible orbits constitute a set of special orbits whose orbital period $T$ is synchronized with the period $T = 2\pi/\omega$ of a rotating frame [27]

$$N_p T = N_d \frac{2\pi}{\omega} \tag{1}$$

where $N_p$ and $N_d$ are two integers and $\omega$ is the angular velocity of the reference frame. For different values of $N_p$ and $N_d$, there is a value of $\omega$ providing the same orbital period. This means that a compatible orbit is also compatible with an infinite set of rotating reference frames. Once that $N_p$ and $N_d$ are chosen, the orbital period of the satellite can be computed from (1), whereas the semimajor axis $a$ is derived from the inversion of the third Keplerian law

$$T = 2\pi\sqrt{\frac{a^3}{\mu}} \tag{2}$$

where $\mu$ is the Earth's gravitational parameter (i.e., the product of gravitational constant and Earth mass) [22].

An FC is a set of spacecrafts running on the same relative trajectory (same repeating space track), a property obtained through a suitable phasing scheme. In order to obtain this property, all the satellites of an FC have common values of the semimajor axis $a$, eccentricity $e$, inclination $i$, and argument $\omega$ of the perigee, while the Right Ascension of the Ascending Node (RAAN) $\Omega_k$ and mean anomaly $M_k$ values for the $k$th satellites must satisfy the following phasing rules [28]:

$$\begin{cases} \Omega_{k+1} = \Omega_k + 2\pi\frac{F_n}{F_d} \\ M_{k+1} = M_k + 2\pi\frac{F_n N_p + F_d F_h}{F_d N_d} \end{cases} \tag{3}$$

where $F_n$, $F_d$, and $F_h$ are three integers ruling the satellite phasing. This means that FCs are characterized by six integers and five orbit Keplerian parameters, i.e., $N_p$ is the number of petals (integer, $N_p > 0$), $N_d$ is the number of days needed to cover the whole closed-loop track (integer, $N_d > 0$), $N_s$ is the number of satellites (integer, $N_s > 0$), $F_n$ is the phase numerator (integer, $F_n > 0$), $F_d$ is the phase denominator (integer $> 0$), $F_h$ is the phasing step (integer, $0 \leq F_h < N_d$), $h_p$ is the perigee altitude ($h_p > h_{p\min}$), $i$ is the inclination ($0 \leq i < \pi$), $\omega$ is the argument of perigee ($0 \leq \omega < 2\pi$), $\Omega_0$ is the RAAN of the first satellite ($0 \leq \Omega_0 < 2\pi$), and $M_0$ is the mean anomaly of the first satellite at epoch time ($0 \leq M_0 < 2\pi$). The first two integers $(N_p, N_d)$ define the semimajor axis (or the orbital period), whereas the last three integers $(F_n, F_d, F_h)$ define the satellite distribution/sequence along the relative path. The Keplerian parameters define the orbit shape, orientation, and synchronization with the Earth (note that assigning $h_p$ is equivalent to assigning the orbit eccentricity $e$). The number of orbits is determined by the $N_p$ parameter, and all the orbits have identical shape, inclination, and argument of perigee. They are only rotated in RAAN to obtain an even distribution about the central body.

The FC approach provides great flexibility and interesting dynamics that reveal the presence of the *Harmonic* FCs (previously called "secondary paths"), a novel space (rigid) object, where the dynamics of the satellites form an object whose shape is time-invariant [27]. The resulting satellites' relative motion results in intriguing motion patterns that can be exploited to obtain useful properties. Evolutionary algorithms can be exploited to optimize FCs with respect to mission-analysis requirements [30], [37].

### B. Optimal FC

The optimal design of an FC requires an optimality definition criterion that can be implemented into a cost function. Constraints on FC design come from the sensor specifications, the satellite-orbit limitations, and the sensor swath (which both influence the spatial resolution and observation repeat time). The scientific requirements on ground spatial resolution and swath imply an orbit height range of 450–1250 km in order to have an average linear FOV of less than 25 km (see also Sections IV and V). The swath has been derived by assuming a spaceborne-radiometer scanning between $\pm 50^\circ$ around the antenna boresight (note that, for constellation design, the channel FOV is not a driving specification). Another major concern is the choice of the inclination angle $i$ which might be chosen either to be a generic freedom parameter or to satisfy Sun-synchronicity or to keep a constant perigee argument (i.e., $i = 63.4^\circ$). The latter choice implies that no perigee-argument correction control is needed.

Several configurations have been foreseen for a systematic mission analysis, supposing a number of satellites less than or equal to four.

1) SS-CO constellation with all satellites equally distributed along the same orbit plane similar to COSMO-SkyMed mission [38]. COSMO-SkyMed is a Walker (WK) constellation [39] with one orbital plane and with four satellites evenly spaced on an SS orbit at an altitude of 622 km (hence, with an inclination of 97.86°) and with a longitude of the ascending node of 274.5°.
2) WK of COs (WK-CO) in different orbital planes with $i = 63.4^\circ$, following the design concept of Walker [39].
3) Two FCs at $i = 63.4^\circ$, one having *slightly* elliptical (FC-SE) orbits with perigee/apogee ratio equal to about 450/850 km, the other one having *moderately* elliptical (FC-ME) orbits with perigee/apogee ratio equal to about 600/1250 km.
4) One FC-SS orbits constellation with different orbital plane for each satellite.

Focusing on a *Mesoscale Western Mediterranean* (MWM) window, defined between $35^\circ/50^\circ$ latitude and $3^\circ/23^\circ$ longitude (see Fig. 1, area bounded by cyan dashed line), we have introduced the *target-area revisit-time interval or gap-time* $\Delta T_{\rm rev}$ as the time interval between two satellite overpasses over the target area, counted when the sensor swath of any constellation satellite intersects the target area. The revisit-time interval is the metrics that drives the constellation-optimization process;

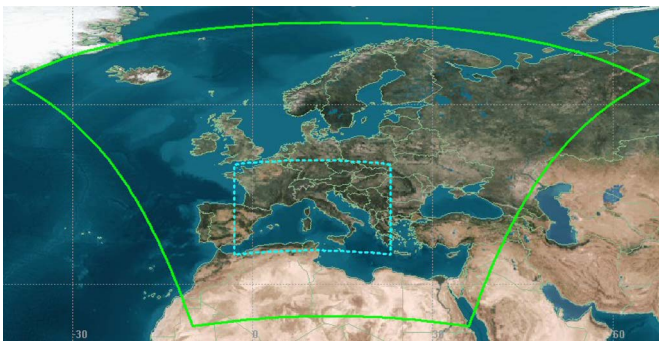

Fig. 1. (Bounded by cyan dashed line) MWM window and (bounded by green solid line) RSE window used as target areas for FLORAD mission analysis optimization.

in particular, we have imposed that the cumulative distribution function (CDF) of the gap time should be lower than 2 h for the third quartile (75% of the time). The coverage analysis has also been extended, considering a larger area at regional scale, named *Regional Scale European* (RSE) window, a spherical cap delimited by the following latitude/longitude corners, respectively: $23^\circ/-10^\circ$, $64^\circ/-40^\circ$, $64^\circ/66^\circ$, and $23^\circ/36^\circ$ (see Fig. 1, area bounded by green solid line).

The first analysis on constellation configurations has been focused on the comparison between the FC-SE and WK-CO using four satellites. The perigee altitude of FC-SE has been bounded to 450–500 km, whereas its apogee has been bounded to 800–900 km. The corresponding WK satellite-orbit altitude has been set equal to the FC-SE medium altitude equal to 661 km with four orbit planes and interplane spacing (i.e., the number of angular slots, given by $360^\circ$ divided by the number of satellites, between the first vehicle in adjacent planes) equal to one [39]. For both FC-SE and WK-CO, the inclination has been set to $63.4^\circ$. This "critical" inclination value satisfies both the need for no perigee control (for elliptical orbits) and the need to focus the mission coverage on the Mediterranean latitudes (the FC apogee is fixed over Mediterranean latitudes).

The optimization results of the FC-SE are reported in Tables I and II in terms of 11 FC and 6 orbital parameters for each satellite; the perigee/apogee ratio is equal to 476/841. The gap-time CDF is shown in Fig. 2. The average revisit time is 54.6 min for the WK, whereas it is 51.1 min for FC. At 75% CDF percentile, the FC-SE provides a performance comparable to WK-CO; a result that is not surprising as the FC ellipticity is almost negligible.

A further analysis has been performed considering the FC-ME orbits with orbit heights between 600 and 1250 km using only three satellites. It is appealing to decrease the number of satellites in order to reduce the project overall system requirements, being confident that the higher altitude will enhance revisit time (the radiometer FOV is wider with respect to lower satellite altitudes), compensating the lower number of satellites with respect to the FC-SE previously analyzed. The perigee altitude has been bounded to 550–650 km, whereas the apogee one has been bounded to 1150–1250 km. The optimization results are reported in Tables III and IV, analogous to Tables I and II, respectively, the ratio of perigee/apogee being 624/1224. As shown in Fig. 3, the FC-ME and FC-SE provide the same level of performance in terms of gap-time CDF with an average revisit time of 56.6 min. This is expected as the lower number of satellites is well compensated by the higher orbit altitude. These results confirm that, using only three satellites, a comparable revisit time can be ensured. On the other hand, it should be noted that the choice of FC-ME implies a degradation of spatial radiometric sensor resolution with respect to lower orbit constellation.

In order to complete the analysis on the FC-ME, time to obtain a global-scale coverage between $-63.4^\circ$ and $+63.4^\circ$ latitudes has been computed. The minimum, maximum, and average time-period values have been computed for two different spatial slices, obtaining the following results: 1) minimum time-period of 4.2 and 1.4 h, respectively, for latitudes lower and higher than $\pm 31^\circ$; 2) average time-period of 6.4 and 4.1 h, respectively, for latitudes lower and higher than $\pm 31^\circ$; and 3) maximum time-period value of 11.2 and 6.4 h, respectively, for latitudes lower and higher than $\pm 31^\circ$. It is worth underlying that the revisit-time CDF results are related to the criterion we adopted before. If different criteria to compute $\Delta T_{\mathrm{rev}}$ are employed (e.g., intersection of the sensor nadir track with the target area) or the target area is modified, the revisit-time statistics will correspondingly change, as it will be shown later on.

The traditional orbit for meteorological satellites is SS, preferred on the basis of favorable observation and satellite solar-illumination requirements (which can have impacts on thermal and power subsystems). For this intercomparison, the FC-SS has been designed in order to have three satellites and an altitude of 1170 km. The FC-SS satellite parameters are reported in Table V. FC-SS is compared with SS-CO, designed in order to have orbits similar to COSMO-SkyMed ones with three satellites equally spaced along the same orbital plane. Gap-time CDF results for FC-SE, SS-CO, and FC-SS are shown in Fig. 4. The SS-CO revisit-time performance is not comparable to the ones provided by the two FCs due to the fact that all satellites share the same orbital plane. FS-SS exhibits performances worse than FC-SE, particularly looking at CDF quartiles larger than 50%. Furthermore, the requirement of maintaining the revisit time lower than 2 h for the third quartile is not satisfied by FC-SS.

A further analysis has been performed in order to quantify orbital perturbations: Both Flower-constellation FC-ME and FC-SS satellite trajectories have been propagated, considering no orbit control. The mission-scenario parameters considered during this analysis are as follows: 1) satellites' area/mass ratio of 0.01 $\mathrm{m}^2/\mathrm{kg}$; 2) satellite mass of 200 kg; 3) drag coefficient of 2.2; 4) average solar radio flux, F10.7 (defined as average solar flux measured at 10.7-cm wavelength), of 180 solar-flux-units (with SFU $= 10^{-22}\ \mathrm{W}\cdot\mathrm{m}^{-2}\cdot\mathrm{Hz}^{-1}$); and 5) geomagnetic index of eight [25]. A worst case analysis has been performed, considering a launch date on 2011, the peak of solar activity, and the mission lifetime between 2011 and 2013. The results are shown in Fig. 5 for FC-ME; results for FC-SS are quite similar. Both FC constellations go through a progressive degradation of performance as time increases even though CDF is always less than 2 h. These results show that constellation orbit control may be avoided for the FLORAD mission, thus implying a propellant saving due to a reduced

TABLE I
FC PARAMETERS FOR AN FC-SE

| $N_p$ | $N_d$ | $N_s$ | $F_n$ | $F_d$ | $F_h$ | $h_p$ (km) | $i$ (deg) | $\omega$ (deg) | RAAN (deg) | $M_0$ (deg) |
|---|---|---|---|---|---|---|---|---|---|---|
| 44 | 3 | 4 | 1 | 4 | 1 | 476 | 63.4 | 251.7 | 282.6 | 287.6 |

TABLE II
SE ORBIT ELEMENTS FOR FOUR SATELLITES FC (FC-SE)

| Sat. N. | Semim. Axis | Ecc. e | $i$ (deg) | $\omega$(deg) | RAAN (deg) | $M_0$ (deg) |
|---|---|---|---|---|---|---|
| 1 | 7037.023 | 0.0259 | 63.42 | 251.74 | 282.68 | 287.66 |
| 2 | 7037.023 | 0.0259 | 63.42 | 251.74 | 192.63 | 287.66 |
| 3 | 7037.023 | 0.0259 | 63.42 | 251.74 | 102.59 | 287.66 |
| 4 | 7037.023 | 0.0259 | 63.42 | 251.74 | 125.48 | 287.66 |

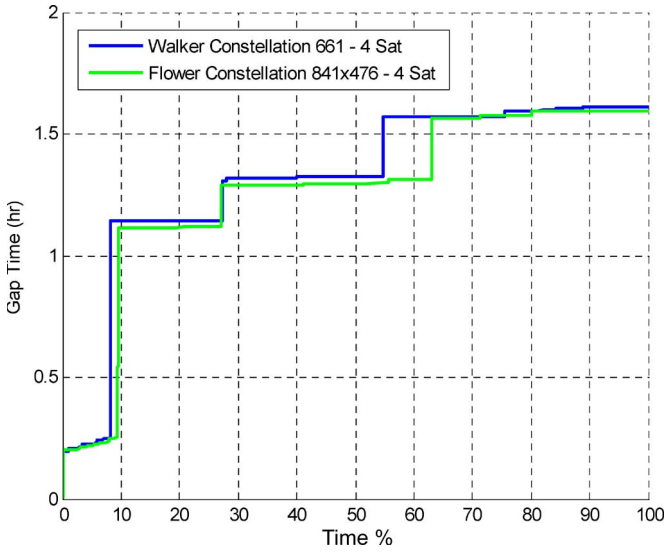


Fig. 2. Gap-time CDF of FC-SE and WK-CO using four satellites for the MWM window of Fig. 1.

number of requested maneuvers. Furthermore, minor changes to the satellites' orbital parameters could be investigated in order to exploit high Earth gravitational-field harmonics to guarantee a long-term repeating ground track without orbit.

A final evaluation is related to the impact of the extension of the target geographical area. Fig. 6 shows a comparison of the gap-time CDF for FC-ME with three satellites, FC-SE with four satellites, FC-SS with three satellites, and WK-CO with four satellites given the RSE window. As expected, when the coverage is enlarged from mesoscale to regional scale, the performances of the designed constellations become comparable being the FCs optimized for Mediterranean latitudes. Furthermore, due to the fact that the European coverage area is wider than the Mediterranean one, the gap time CDF at 75% is below 1.5 h for all constellations.

### C. Constellation Launching Strategies

Multiple launches may strongly affect the appealing features of a small mission [25]. However, placing in orbit a minisatellite constellation with only one launch requests a careful plan. The most appealing option may represent an appealing tradeoff between constellation deployment time and propellant load, needed for orbit maneuvers. The concept is based on the Hohmann transfer orbit technique (usually used to place in orbit geostationary satellites) and the precession of RAAN ($\Omega$), expressed by [22]

$$\frac{d\Omega}{dt} = \frac{dM}{dt}\left[\frac{3}{2}J_2\left(\frac{r_{eq}}{a}\right)^2(1-e^2)^{-2}\cos i\right] \tag{4}$$

where $M$ is the mean anomaly, $J_2$ is the second-harmonic coefficient of the Earth gravitational-field expansion, $a$ is the semimajor axis, and $r_{eq}$ is the mean Earth radius. By exploiting the dependence of the RAAN precession with respect to orbit height, after the injection of the $N_s$ satellite into the same elliptical orbit, each satellite-orbit plane is modified by changing its orbit height.

From (4) and considering the FC-ME configuration, it emerges that this launch with a transfer to about 2000 km would request about 125 days for a relative drift of 120° and about 220 days for a relative drift of 240°. If the first satellite can be deployed into its elliptical orbit during the launcher descend, the deployment of a three-satellite constellation should take about seven months. To a first approximation, less than 60 kg of propulsion monopropellant may be needed to accomplish the satellite descending maneuvers [25].

## IV. DESIGN OF FLORAD MMW RADIOMETER

A compact MMW radiometer needs a careful selection of the channel number and their central frequency. Within the FLORAD payload concept, low-frequency MW channels may have a major impact on the size and weight [22], [32], [33]. This drives toward the selection of channels above W-band, more specifically above 80 GHz. This choice may be limiting for the observation of near-surface parameters but does not degrade too much the overall performance of the mission with respect to its scientific objectives. On the other hand, MMW technology above 250 GHz is currently not in a mature stage for space deployment. This means that choosing frequencies above 250 GHz may result to be too costly for a small space mission. Moreover, temperature and humidity may be easily sensed using absorbing frequency bands below 250 GHz [2], [4]. Of course, AMSU, MHS, SSM/IS, and Advance Microwave Scanning Radiometer spaceborne-radiometer legacy is another constraint to keep in mind, particularly for climate-record applications. Due to its foreseen scanning capability, the FLORAD payload has been named FLORAD MMW Imaging Sounder (FLOMIS).

### A. Selection of FLOMIS Channels

In order to define the FLOMIS-channel configuration, a set of candidates have been ranked by performing a sequential channel selection on a globally representative database of simulated atmospheric profile. The channel selection performs a ranking according to the contribution that a given observation (a radiometric channel in this case) brings to the knowledge of a particular atmospheric state, based on the concepts of

TABLE III
SAME AS IN TABLE I BUT FOR A THREE-SATELLITE FC-ME

| $N_p$ | $N_d$ | $N_s$ | $F_n$ | $F_d$ | $F_h$ | $h_p$ (km) | $i$ (deg) | $\omega$ (deg) | RAAN (deg) | $M_0$ (deg) |
|---|---|---|---|---|---|---|---|---|---|---|
| 8 | 8 | 3 | 1 | 3 | 3 | 624 | 63.42 | 265.97 | 60.27 | 63.59 |

TABLE IV
SAME AS IN TABLE II BUT FOR A THREE-SATELLITE FC-ME

| Sat. N. | Semim. Axis | Ecc. e | $i$ (deg) | $\omega$ (deg) | RAAN (deg) | $M_0$ (deg) |
|---|---|---|---|---|---|---|
| 1 | 7302.2149 | 0.0410 | 63.42 | 265.97 | 60.27 | 63.59 |
| 2 | 7302.2149 | 0.0410 | 63.42 | 265.97 | 180.33 | 63.59 |
| 3 | 7302.2149 | 0.0410 | 63.42 | 265.97 | 300.39 | 63.59 |

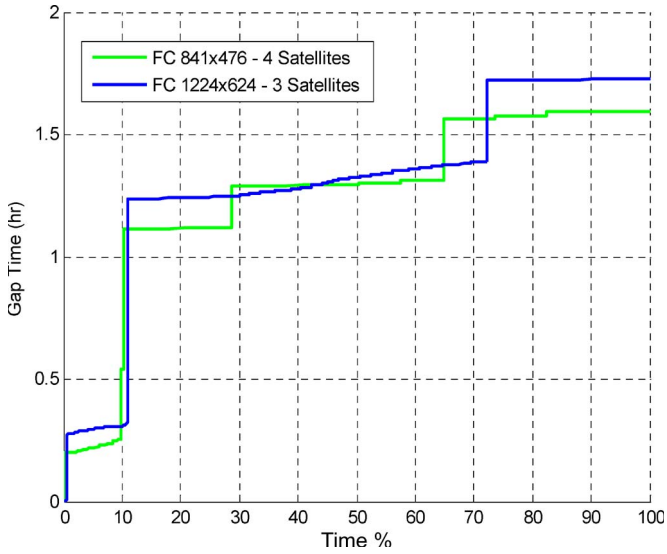


Fig. 3. As in Fig. 2 but for FC-SE with four satellites and FC-ME with three satellites.

information and optimal estimation theory [31]. In the following, the state of the atmosphere (in this paper, atmospheric profiles to be retrieved) is denoted as a vector $\mathbf{x}$, and the multiple-channel radiometric observations are contained in a vector $\mathbf{y}$. The physical link between $\mathbf{x}$ and $\mathbf{y}$ is described by the radiative-transfer (RT) observation operator $H$ that may be nonlinear. The modeled observations $\boldsymbol{y}$ are as follows:

$$\mathbf{y} = H(\mathbf{x}) + \boldsymbol{\varepsilon} \tag{5}$$

where $\varepsilon$ summarizes observation errors (e.g., radiometer noise) and forward modeling errors (e.g., RT model uncertainties).

The optimal estimation theory also requires the knowledge of the *a priori* information on the state vector $\mathbf{x}_b$. If the problem is supposed to be only weakly nonlinear, the simulation can be written as

$$\mathbf{y} = H(\mathbf{x}_b) + \mathbf{H}(\mathbf{x} - \mathbf{x}_b) + \boldsymbol{\varepsilon} \tag{6}$$

which corresponds to the first-order Taylor development with the tangent-linear approximation $\mathbf{H}$ of the forward model $H$. The condition that the forward model behaves linearly can be realistic even for clouds and precipitation if $\mathbf{x}_b$ is close enough to the true state. By definition in a Bayesian context, a solution is optimal when $p(\mathbf{x}|\mathbf{y})$, the posterior probability density function (PDF), is maximized. For linear applications, the Bayesian theory reduces to the optimal estimation theory [31]. Under the further assumptions of Gaussian statistics for $\mathbf{x}$ (centered around $\mathbf{x}_b$ and with error covariance matrix $\mathbf{B}_\varepsilon$) and for $\boldsymbol{\varepsilon}$ (with zero mean and error covariance $\mathbf{C}_\varepsilon$,), it can be shown that the optimal analysis $\hat{\mathbf{x}}$ of the state $\mathbf{x}$ has the following expression [31]:

$$\hat{\mathbf{x}} = \mathbf{x}_b + \mathbf{A}_\varepsilon \mathbf{H}^{\mathrm{T}} \mathbf{C}_\varepsilon^{-1} [\mathbf{y} - \mathbf{H}\mathbf{x}_b] \tag{7}$$

with $\mathbf{H}^{\mathrm{T}} = \delta H / \delta \mathbf{x}$ as the adjoint of the observation operator (expressed in terms of Frechet derivative) and $\mathbf{A}_\varepsilon$ as the *analysis-error covariance matrix*, defined as

$$\mathbf{A}_\varepsilon = \left(\mathbf{B}_\varepsilon^{-1} - \mathbf{H}^{\mathrm{T}} \mathbf{C}_\varepsilon^{-1} \mathbf{H}\right)^{-1}. \tag{8}$$

The information content of an observation is a quantitative measure of the reduction of the estimation error produced by the observation. The improvement of estimation error depends on the sensitivity of the observation $\mathbf{y}$ to the state $\mathbf{x}$ and on the accuracy of the measurement and modeling, i.e., on $\mathbf{H}$ and $\mathbf{C}_\varepsilon$, their respective magnitudes, and, finally, on the accuracy of the *a priori* information (through $\mathbf{B}_\varepsilon$). This makes the information content similar to the signal-to-noise ratio.

There have been several formulations of the information content. The entropy reduction (ER) [40] is defined as the difference between the entropy of the *a priori* PDF $\mathrm{p}(\mathbf{x})$ and the one of the *a posteriori* probability $\mathrm{p}(\mathbf{x}|\mathbf{y})$

$$\mathrm{ER} = E\left[p(\mathbf{x})\right] - E\left[p(\mathbf{x}|\mathbf{y})\right] = \frac{1}{2}\log_2\left[\frac{|\mathbf{B}_\varepsilon|}{|\mathbf{A}_\varepsilon|}\right] \tag{9}$$

where $|\sim|$ indicates the determinant operator. The right-hand side of (9) holds under the assumption of Gaussian distribution. The log with basis "2" is usually chosen for expressing ER in units of bits.

The actual channel selection is an iterative procedure proposed by Rodgers [41] in which the contribution of each channel is sequentially quantified based on the hypothesis of error uncorrelation among channels, i.e., that $\mathbf{C}_\varepsilon$ is diagonal. Iterative methods loop over channels and sort them by decreasing information content given *a priori* information (from the model background $\mathbf{B}_\varepsilon$) and that from the ones previously selected. Given a set of candidate channels, the iterative-selection method starts with no channels selected and, sequentially, chooses the channel with the highest information content, taking into account the information provided by previously selected channels. Therefore, at each iteration, (9) requires an update to the error covariance matrix $\mathbf{A}_\varepsilon$ (initially, $\mathbf{A}_{\varepsilon 0} = \mathbf{B}_\varepsilon$).

TABLE V
SAME AS IN TABLE II BUT FOR A THREE-SATELLITE FC-SS

| *Sat. N.* | *Semim. Axis* | *Ecc. e* | *i (deg)* | *ω (deg)* | *RAAN (deg)* | *$M_0$ (deg)* |
|---|---|---|---|---|---|---|
| 1 | 7549.0792 | 3.2082e-005 | 100.34 | 0 | 6.99 | 0 |
| 2 | 7549.0792 | 3.2082e-005 | 100.34 | 0 | 127.05 | 0 |
| 3 | 7549.0792 | 3.2082e-005 | 100.34 | 0 | 247.11 | 0 |

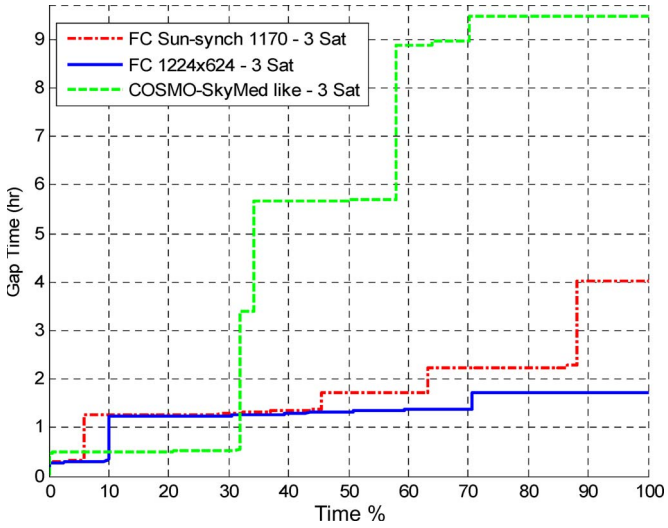


Fig. 4. Gap-time CDF of FC-ME, FC-SS, and one-orbit-plane COSMO-like constellation using three satellites for the MWM target area of Fig. 1.

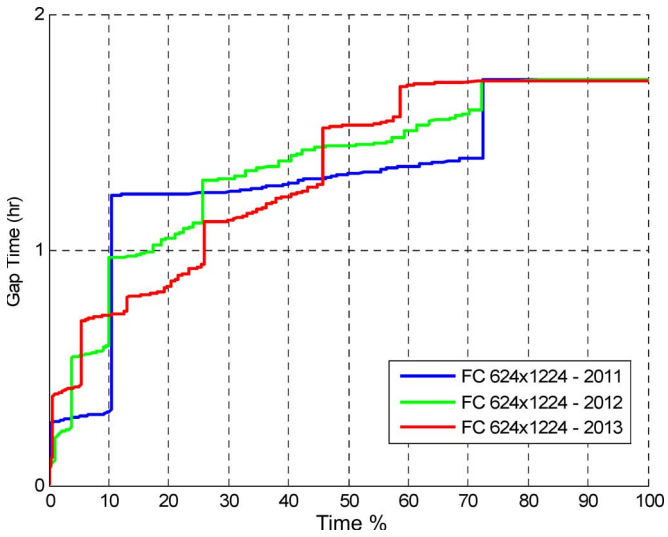


Fig. 5. Degradation of gap-time CDF for FC-ME considering orbital perturbation during three years of operation (starting on 2011) for the MWM target area of Fig. 1.

The difference of $\mathbf{A}_\varepsilon$ between two iteration steps $k$ and $k-1$ determines the information gain or reduction of ER ($\Delta$ER) [40]

$$\Delta \mathrm{ER} = \frac{1}{2}\log_2\left[\frac{|\mathbf{A}_\varepsilon(k-1)|}{|\mathbf{A}_\varepsilon(k)|}\right]. \tag{10}$$

The iteration procedure may be terminated when all channels have been selected or the information content of additional channels reaches a certain threshold (details on this procedure are given in [40]).

In order to perform the ER analysis, atmospheric profiles were extracted from the ECMWF forecasting system with

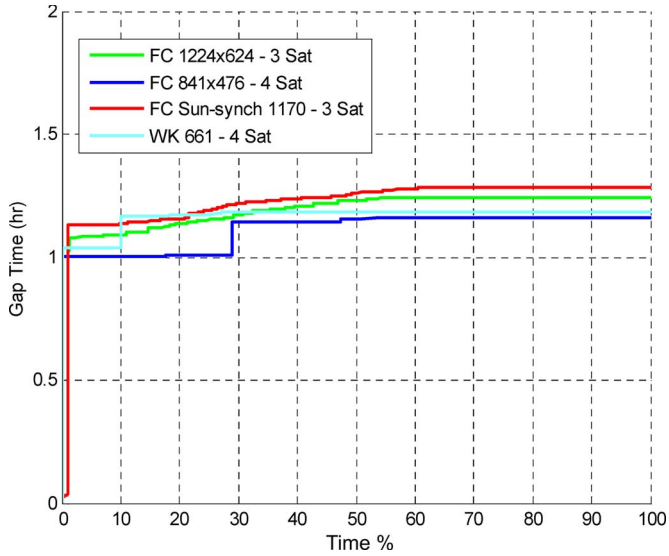


Fig. 6. Same as Fig. 1 but comparing FC-ME with three satellites, FC-SE with four satellites, FC-SS with three satellites, and WK-CO with four satellites for the RSE window.

horizontal resolution close to 25 km [42]. Vertical resolution is achieved using 91 pressure levels. Forecasts containing all geophysical parameters needed to apply RT, relative to 36-, 42-, 48-, and 54-h ranges of day 1, 10, and 20 of every month between July 2006 and June 2007 were used. To avoid excessive computation due to about 121 million profiles, the original samples were reduced by a random resampling into uniform distributions. To guarantee a geographically global coverage, the sampling was performed separately over profiles located into grid boxes of 15° by 10°. Separate sampling was repeated for profiles with different time of the day and month to keep the meteorological representativeness. Two data sets were eventually built: The first containing cloudy (but not precipitating) profiles and the second composed only of precipitating profiles [8]. The total number of used profiles is 220 627 (i.e., 147 472 precipitating, 73 155 nonprecipitating and 146 203 over ocean, 74 424 over land). The first one was also used for the channel selection in clear-sky conditions (setting cloud variables to zero). If $z_i$ are the altitude discrete levels with $i = 1 - N_z$, the atmospheric state vector $\mathbf{x}$ is then represented by the temperature vertical profile $T(z_\mathrm{i})$ [in Kelvin], water-vapor vertical profile $V(z_\mathrm{i})$, nonprecipitating (cloud) water-content vertical profile $W_c(z_\mathrm{i})$, precipitating (rain) water-content vertical profile $W_r(z_\mathrm{i})$, nonprecipitating (ice crystals and aggregates) solid-water-content vertical profile $W_i(z_\mathrm{i})$, and precipitating (snow and graupel) solid-water-content vertical profile $W_s(z_\mathrm{i})$.

The observation operator $H$ consists of an RT model that accounts for both absorption and multiple scattering at MW frequencies in clouds and precipitation, based on the Eddington approximation [43], [44]. The background error covariance $\mathbf{B}_\varepsilon$

TABLE VI
PRIORITY RANKING OF MMW FREQUENCY CHANNEL FOR TROPOSPHERIC PARAMETER RETRIEVAL FOR CROSS-TRACK LS AND CS USING 89–230-GHz FREQUENCY RANGE

| ER Priority | Water vapor over Ocean | | Water vapor over Land | Temperature over Ocean | | Temperature over Land | | Clouds | | Clouds and Precipitation | |
|---|---|---|---|---|---|---|---|---|---|---|---|
| | Clear Sky | Cloudy | | Clear Sky | Cloudy | Clear Sky | Cloudy | Ocean | Land | Ocean | Land |
| Radiometer Linear Scanning (LS) | | | | | | | | | | | |
| 1 | 183.31±1.8 | 183.31±1.8 | 183.31±1.8 | 118.75±1.1 | 118.75±0.7 | 118.75±0.7 | 118.75±0.7 | 89.0 | 229.0 | 118.75±2.1 | 118.75±2.1 |
| 2 | 183.31±3.0 | 183.31±1.0 | 183.31±3.0 | 118.75±5.0 | 118.75±1.1 | 118.75±1.1 | 118.75±1.1 | 118.75±5.0 | 118.75±3.0 | 89.0 | 118.75±5.0 |
| 3 | 183.31±4.5 | 183.31±3.0 | 183.31±1.0 | 118.75±3.0 | 118.75±3.0 | 118.75±1.5 | 118.75±1.5 | 118.75±3.0 | 118.75±5.0 | 118.75±5.0 | 118.75±3.0 |
| 4 | 183.31±1.0 | 183.31±7.0 | 183.31±4.5 | 118.75±2.1 | 118.75±2.1 | 118.75±2.1 | 118.75±2.1 | 118.75±2.1 | 118.75±1.5 | 118.75±3.0 | 118.75±1.5 |
| 5 | 183.31±7.0 | 183.31±4.5 | 183.31±7.0 | 118.75±0.7 | 118.75±1.5 | 118.75±3.0 | 118.75±3.0 | 118.75±1.5 | 166.0 | 118.75±1.5 | 166.0 |
| Radiometer Conical Scanning (CS) | | | | | | | | | | | |
| 1 | 183.31±1.8 | 183.31±1.8 | 183.31±1.8 | 118.75±0.7 | 118.75±0.7 | 118.75±0.7 | 118.75±0.7 | 89.0 | 118.75±2.1 | 118.75±2.1 | 118.75±2.1 |
| 2 | 183.31±3.0 | 183.31±1.0 | 183.31±1.0 | 118.75±1.1 | 118.75±1.1 | 118.75±1.1 | 118.75±1.1 | 118.75±3.0 | 89.0 | 118.75±3.0 | 118.75±3.0 |
| 3 | 183.31±4.5 | 183.31±3.0 | 183.31±3.0 | 118.75±1.5 | 118.75±1.5 | 118.75±1.5 | 118.75±1.5 | 118.75±5.0 | 118.75±5.0 | 118.75±5.0 | 118.75±5.0 |
| 4 | 183.31±1.0 | 183.31±4.5 | 183.31±4.5 | 118.75±2.1 | 118.75±3.0 | 118.75±2.1 | 118.75±3.0 | 118.75±2.1 | 118.75±3.0 | 118.75±1.5 | 118.75±1.5 |
| 5 | 183.31±7.0 | 183.31±7.0 | 183.31±7.0 | 118.75±3.0 | 118.75±2.1 | 118.75±3.0 | 118.75±2.1 | 118.75±1.5 | 118.75±1.5 | 118.75±1.1 | 166.0 |

TABLE VII
FLOMIS RADIOMETER CONFIGURATIONS (H: HORIZONTAL POL., V: VERTICAL POL.); THE ASSUMED ACCURACY IN KELVIN OF EACH CHANNEL IS SHOWN WITHIN PARENTHESIS

| Name | No. channels | FLOMIS frequency channels |
|---|---|---|
| *MHS-like* | *5* | 89V GHz (0.3), 166.0V GHz (0.5), 183.31V±1.0 GHz (0.5), 183.31V ±3.0 GHz (0.5), 190.3V GHz (0.5) |
| *MHTS1* | *8* | 89H GHz (0.3), 89V GHz (0.3), 166.0V GHz (0.5), 118.75V±0.7 GHz (0.75), 118.75V±3.0 GHz (0.5), 183.31V±1.0 GHz (0.5), 183.31V ±3.0 GHz (0.5), 190.3V GHz (0.5) |
| *MHTS2* | *8* | 89H GHz (0.3), 89V GHz (0.3), 118.75V±0.7 GHz (0.75), 118.75V±3.0 GHz (0.75), 183.31V±1.0 GHz (0.5), 183.31V ±3.0 GHz (0.5), 190.3V GHz (0.5), 229.0H GHz (0.5) |
| *MHTS+* | *10* | 89H GHz (0.3), 89V GHz (0.3), 166.0V GHz (0.5), 118.75V±0.7 GHz (0.75), 118.75V±2.1 GHz (0.7), 118.75V±3.0 GHz (0.5), 183.31V±1.0 GHz (0.5), 183.31V ±3.0 GHz (0.5), 190.3V GHz (0.5), 229.0H GHz (0.5) |

for temperature, water vapor, and hydrometeor contents and the total error covariance $\mathbf{C}_\varepsilon$ are computed as in [38]. The measurement vector $\mathbf{y}$ is, in general, represented by the set of $T_{Bp}(v_j, \theta)$ at prescribed frequencies $\nu_j$ with $j = 1 - N_\nu$, polarization $p = 1 - N_p$, and incidence angle $\theta$ plus ancillary measurements $m_l$ with $l = 1 - N_a$ such as available surface data from conventional meteonetworks and/or forecast numerical models.

The ER-based channel-selection methodology has been applied to FLOMIS specifications, choosing a starting set of frequency channels between 90 and 230 GHz at vertical and horizontal polarization, starting from the Post-EPS frequency set for future MW sounder and imager [8], [23]. The final ranking of the considered frequency set is done, evaluating an average $\Delta$ER on all the profiles of the data set. Table VI summarizes the results. This table is subdivided for each tropospheric parameter of interest, i.e., humidity, temperature, clouds, and precipitation. Moreover, both land and ocean surface cases are distinguished, whereas humidity and temperature results are also separated for cloudy and clear sky. Both cross-track linear scanning (LS) at nadir pointing and conical scan (CS) at 53° off-nadir angle are also considered. Dual-sideband channels are also considered in Table VI, even though the bandwidth effect is neglected.

As expected, having excluded 50/60-GHz channels, the ones in the 118-GHz absorption band are the most sensitive to tropospheric temperature. Channels in the 183-GHz band are the most suitable for water-vapor retrieval, and it resulted that they rank the highest even if 23.8 GHz would be included among the candidates. In general terms, we note that, for both water vapor and temperature, the more opaque channels are preferred in cloudy conditions and over land; comparing the results for LS with the ones for CS, we also note that the viewing angle (0° and 53°, in this case) affects the ranking only in clear sky over ocean. For clouds and precipitation, 89, 166, and 229 GHz play the main role together with the optically more transparent channels in the 118-GHz band.

### B. Case-Study Analysis of FLOMIS Configurations

In order to perform a numerical test of various FLOMIS configurations over the mesoscale region of interest (see Fig. 1), we have selected a case study using the output of a mesoscale NWP model (e.g., [9], [11], and [18]). Thermodynamical and water-content input profiles have been taken from the Mesoscale Model version 5 (MM5) from Pennsylvania State University and National Center for Atmospheric Research [45]. The selected case study on October 10, 2007 within the MWM target area was simulated through MM5 with 33 vertical levels, 27-km spatial resolution in the region with latitudes between $35°/50°$ and longitudes between $-3°/23°$. During that period, a mesoscale convective system was developed in central Italy, and it lasted for few days.

For this case study, we have implemented various FLOMIS configurations to perform tropospheric-profile retrieval as in Table VII. Table VII lists the frequency set deduced from the ER-based analysis given in Table VI. Four configurations have been considered: 1) MHS-*like* resembles the five-channel set available on MHS [33]; 2) Microwave Humidity and Temperature Sounder-1 (MHTS1) includes in addition another polarization at 89 GHz and two channels around the 118-GHz

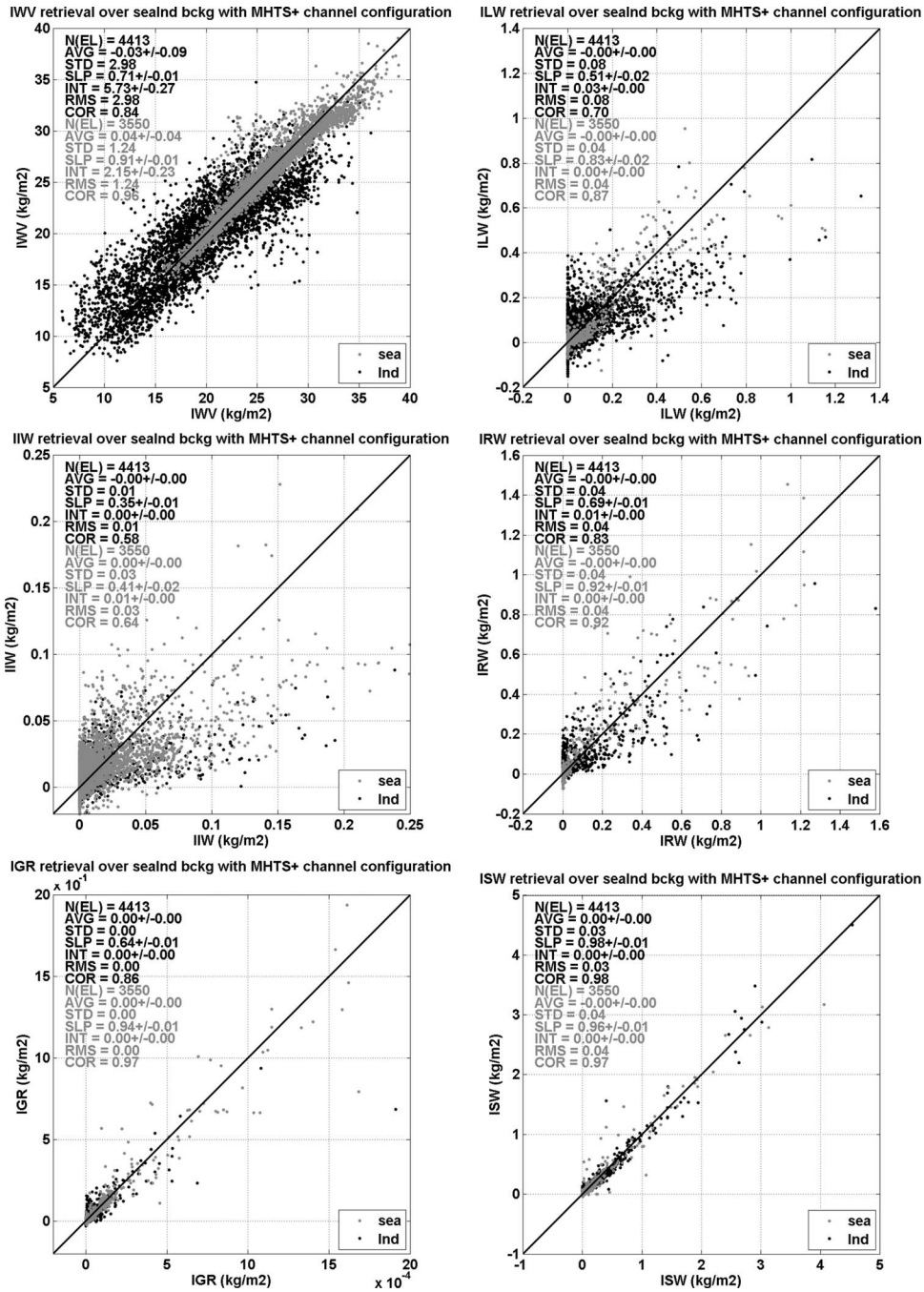


Fig. 7. Scatter plots of IWV, ILW, IIW, IRW, IGR, and ISW retrieved from simulated MHTS+ observations over (gray) ocean and (black) land backgrounds and compared with corresponding modeled values (on abscissas). The error statistics are given in text using the corresponding color.

oxygen line; 3) MHTS2 is as MHTS1 but deploys the 229-GHz channel instead of 166 GHz; and 4) MTHS+ merges both MHTS1 and MHTS2 configurations and also adds one more channel in the 118-GHz band. Note that, in all configurations, we have included 166 GHz, instead of 157 GHz, since there are indications that higher frequency channel may give better performances than the 157 GHz presently on MHS [40], [46]. An additional reason for preferring 166 GHz is that this frequency is fully protected by the International Telecommunication Union. For this case-study analysis, a CS at 53° incidence angle has been supposed with a uniform channel FOV equal to about 25 km.

The retrieval of the tropospheric parameters, indicated by the $\mathbf{x}$ vector, has been performed by means of two statistical inversion algorithms: 1) multiple regression (MR); 2) maximum likelihood (ML). From (7), MR can be expressed by [31]

$$\hat{\mathbf{x}} = \langle \mathbf{x} \rangle + \mathbf{C}_{xy}\mathbf{C}_{yy}^{-1}\left[\mathbf{y} - \langle \mathbf{y} \rangle\right] \tag{11}$$

where $\mathbf{C}_{xy}$ is the cross covariance between $\mathbf{x}$ and $\mathbf{y}$, $\mathbf{C}_{yy}$ is the autocovariance of $y$, and angle brackets indicate ensemble average. For our purposes, we have employed a polynomial regression model of third order in $T_{Bp}$ both for profile- and integrated-content retrieval.

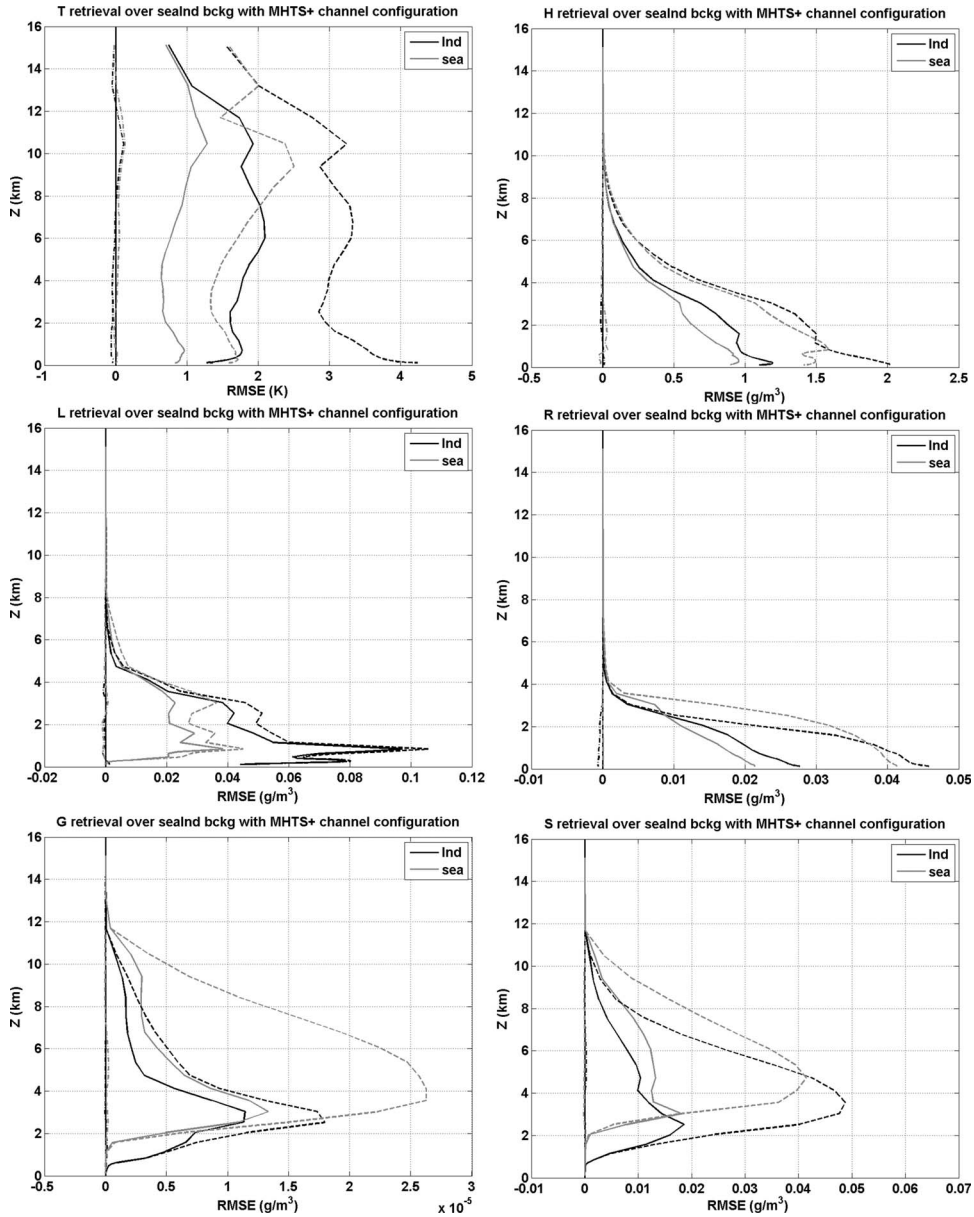


Fig. 8. Profiles of rmse for atmospheric variables retrieved over (gray) ocean and (black) land backgrounds (T: temperature, H: humidity, L: cloud liquid, R: rain, G: graupel, S: snow). (Dashed) Corresponding variability (standard deviation over the whole set) is also shown.

The ML algorithm can be deduced from (5) where the error is supposedly Gaussian. Then, the retrieved parameter is obtained by minimizing the error distance with respect to $\mathbf{x}$ (e.g., [14] and [16])

$$\hat{\mathbf{x}} = \min_{\mathbf{x}} \left[ (\mathbf{y} - H(\mathbf{x}))^{\mathrm{T}} \mathbf{C}_{\varepsilon}^{-1} (\mathbf{y} - H(\mathbf{x})) \right] \qquad (12)$$

where $H(\mathbf{x})$ is the simulated $T_{Bp}$ from the state vector $\mathbf{x}$. The inverse method has been trained and tested, dividing the whole data set into two groups (with a sample ratio of $10:1$) according to the different background type (sea and land). The choice of the training set was driven by representing better than a climatological mean the *a priori* information we intend to use in the operational retrieval (1-D variational retrieval method). Random noise was added to simulated $T_{Bp}$ for accounting instrumental noise, and a simple emissivity model was used in computing the upwelling brightness temperatures. For the ocean background, we have used FASTEM V2 parameterization [46], while for land background, the emissivity is calculated by linear interpolation of frequency-dependent estimated values [47]. In this simplified approach, the land surface emissivity has not been considered affected by random uncertainty.

Fig. 7 shows the scatter plots of IWV, liquid water (ILW), ice water (IIW), rain water (IRW), graupel (IGR), and snow water (ISW), retrieved from simulated MHTS+ observations over ocean and land background. The statistics are given in each figure text. For what concerns IWV retrieval, as well known, the MR retrieval accuracy depends on the background type as it is significantly better over sea (i.e., correlation of 0.96) than over land (i.e., correlation of 0.84). The MR results for ILW retrieval show that overall performances are worse than for IWV with correlations less than 0.87 for ocean and 0.70 for land applications. Similar considerations apply for the IIW,

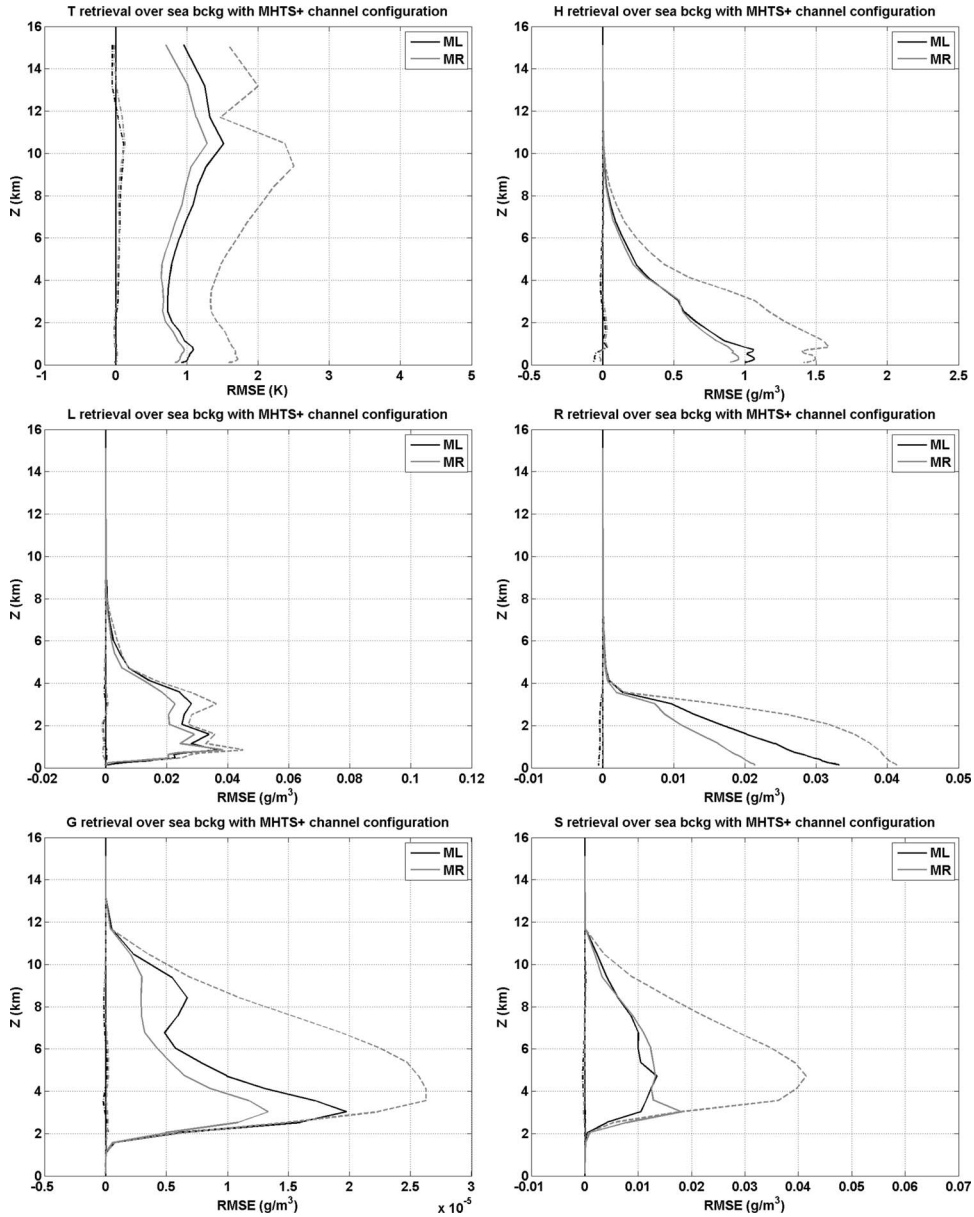


Fig. 9. Profiles of rmse for atmospheric variables retrieved over ocean using ML and MR retrieval algorithms (T: temperature, H: humidity, L: cloud liquid, R: rain, G: graupel, S: snow). (Dashed) Variability of the whole set (standard deviation) is also shown.

IRW, and ISW but with ice retrievals much worse than the others (correlations less than 0.64 over ocean). It is notable that over-ocean correlations are about 0.92 and 0.97 for IRW and ISW, respectively. Fig. 7 shows a small number of samples with IWV $< 10$ kg/m$^2$, suggesting that the case study presents few dry winter cases. The retrieval performances shown in Figs. 7–10 depend slightly on and are strictly valid only for this case study, while more general conclusions should be drawn, examining a global data set, as the one used in Section IV-A.

Fig. 8 shows the profiles of root mean-square error (rmse) for atmospheric variables retrieved from MR over ocean and land background from simulated MHTS+ observations. The corresponding variability, expressed as standard deviation over the whole set, is also shown in order to indicate the information gain due to the use of radiometric observations. The error uncertainty for temperature retrieval over ocean is less than 1 K over ocean and less than 2 K over land (neglecting uncertainties related to surface emissivity). The rmse for humidity profiles is less than 1 g/m$^3$ over ocean and 1.5 g/m$^3$ over land near the surface and it decreases with increasing height. Nonprecipitating liquid and ice profiles are again difficult to retrieve both over land and ocean, but better results are obtained for rain and snow retrieval with errors less than 0.03 and 0.02 g/m$^3$, respectively, both over land and ocean.

Fig. 9 shows the rmse profiles for variables retrieved over ocean using ML and MR with the MHTS+ configuration. The variability of the whole set, in terms of its standard deviation, is also shown. The performances of MR and ML are usually comparable even though the cubic-regression algorithm tends to be more accurate than ML technique, particularly for temperature, rain, and graupel retrievals. These results seem to indicate that the overall retrieval error is only slightly algorithm-dependent.

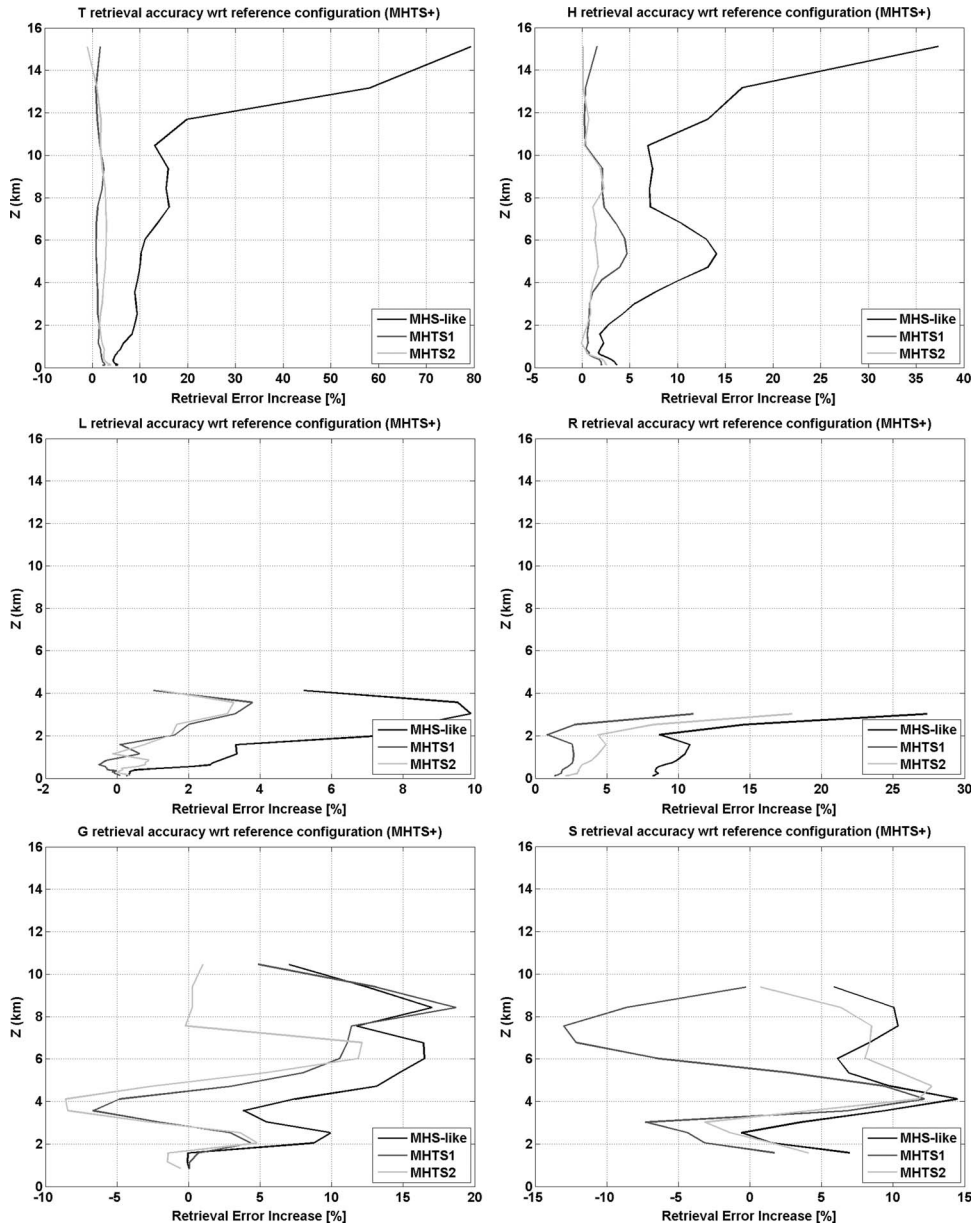


Fig. 10. Percentage increase of profile retrieval error (T: temperature, H: humidity, L: cloud liquid, R: rain, G: graupel, S: snow) using different radiometer configurations with respect to MHTS+, considering the whole data set (both land and ocean backgrounds).

In order to carry out an intercomparison among the various FLOMIS configurations given in Table VII, Fig. 10 shows the percentage fractional increase $f_{\mathrm{rmse}}$ of the profile-retrieval rmse using different configurations (i.e., MHS-like, MHTS1, and MHTS2) with respect to MHTS+, expressed for the whole data set (both land and ocean backgrounds). The index $f_{\mathrm{rmse}}$, depending on the altitude $z$ in case of profile retrieval, is expressed by

$$f_{\mathrm{rmse}} = 100\frac{\mathrm{rmse}_{\mathrm{MHTS+}} - \mathrm{rmse}_{\mathrm{conf}}}{\mathrm{rmse}_{\mathrm{MHTS+}}} \tag{13}$$

where $\mathrm{rmse}_{\mathrm{MHTS+}}$ stands for the rmse due to MHTS+ configuration, whereas $\mathrm{rmse}_{\mathrm{conf}}$ refers to the other considered. This analysis suggests that MHTS+, MHTS1, and MHTS2 are generally better than MHS-like configuration, as expected, particularly for temperature and humidity. Moreover, the fact that $f_{\mathrm{rmse}}$ is larger than 0% indicates that MHTS+ is the best configuration among those considered, even though the results for graupel and snow retrievals also show that MHTS1 may be a competing system solution.

Similarly to Fig. 10, Table VIII shows the fractional error $f_{\mathrm{rmse}}$ for the retrieval of integrated water contents already shown in Fig. 8. For IWV, the improvement of MHTS+ is less than $\sim$2% with respect to MHTS1 and MHTS2 configurations but higher than 4% with respect to MHS-like. Similar considerations hold for nonprecipitating integrated liquid and ice retrievals, even though with larger fractional increases. For precipitating liquid and ice, MHTS+ improvement may be larger than 10%, particularly over ocean.

The importance of the 229-GHz channel is worth a few more words as it is really twofold [46]. In the first place, the scattering

TABLE VIII
PERCENTAGE INCREASE (IN PERCENT) OF COLUMNAR WATER RETRIEVAL ERROR (IWV: INTEGRATED WATER VAPOR, ILW: INTEGRATED LIQUID WATER, IIW: INTEGRATED ICE WATER, IRW: INTEGRATED RAIN WATER, IGW: INTEGRATED GRAUPEL WATER, ISW: INTEGRATED SNOW WATER) USING DIFFERENT CONFIGURATIONS WITH RESPECT TO MHTS+

| Configuration | Background | IWV | ILW | IRW | IIW | IGR | ISW |
|---|---|---|---|---|---|---|---|
| MHS-like | Land | 3.94 | 16.36 | 12.30 | 5.90 | 9.97 | 9.61 |
| MHTS1 | Land | 1.48 | 1.66 | 1.88 | 4.96 | 8.21 | 3.26 |
| MHTS2 | Land | 1.49 | 4.09 | 7.48 | 3.35 | 6.01 | 8.08 |
| MHS-like | Sea | 7.89 | 11.88 | 21.04 | 8.24 | 5.18 | 11.99 |
| MHTS1 | Sea | 0.13 | 1.32 | 3.46 | 8.24 | 1.69 | 11.73 |
| MHTS2 | Sea | 2.16 | 2.31 | 5.74 | 2.77 | 16.87 | 26.09 |

of radiation is quite higher at this frequency than at 89 GHz, offering a method to better detect thin ice clouds as cirrus. This improved capability in detecting cirrus clouds is true also with respect to the window channels currently deployed with MHS (157 and 190 GHz). Moreover, operational observation errors for an MHS-like sounder are currently relatively high, significantly reducing the impact of the data in NWP assimilation. A significant portion of these high errors is related to the presence of undetected cloud in the instantaneous FOV. Thus, there is a feeling that the increased skill at detecting thin cirrus provided by a 229-GHz channel would indirectly reduce the error in the background humidity profile. In practice, a 229-GHz channel should allow more weight to be given to the 183-GHz channels in data assimilation, thus significantly increasing their impact. A recent study demonstrated this aspect and pointed out that adding more channels at 183 GHz cannot give the same result as having the 229-GHz channel [46]. They concluded that the additional 183-GHz channels they used ($183.31 \pm 1.8$ and $\pm 4.5$ GHz) appear to have only marginal positive impact even in cloud-free areas.

## V. DISCUSSION AND CONCLUSION

The FLORAD mission scientific objectives are aimed at the retrieval of thermal and hydrological properties of the troposphere, specifically temperature and water-vapor profiles, cloud liquid content, and rainfall and snowfall. In order to fulfill the goal of a short revisit time for meteorological-monitoring purposes on a quasi-global scale with special focus on a specific target region, an FC of minisatellites has been proposed at pseudogeostationary scale. FC can offer several degrees of freedom in its design, and its features are here discussed. FC launching strategies have been also anticipated. Various configurations of the MMW radiometer multiband channels have been discussed, pointing out the tradeoff between performances and complexity. The optimal frequency set of FLOMIS has been selected on the basis of the ER estimation technique. Both MR and ML retrieval algorithms have been set up to quantify the error budget of each FLOMIS configuration using a case study on the target Mediterranean area.

The results of this numerical analysis may give an idea of the expected performances of the FLORAD mission products, even though based on a single case study and obtained by neglecting the surface-emissivity uncertainty. The latter may be overcome by using clear-air mapping and exploiting the frequent update of the FLORAD constellation overpass. For NWP data-assimilation purposes, FLORAD brightness-temperature measurements can be considered to be a mission product. In this respect, the spaceborne exploitation of the 118-GHz band might represent a unique opportunity, as it has never been tested in space, even though it is foreseen for Post-EPS [23]. The same consideration applies to the 229-GHz band whose role has already been discussed.

Spatial-resolution requirement may be critical at an altitude of about 1200 km when considering FC-ME orbits. However, at 89 GHz, with an antenna of 0.9° half-power beamwidth, the nadir linear FOV would be about 19 km with a cross-track swath about 2000 km (assuming an off-nadir angle of $\pm 50°$). Higher MMW frequency channels would have an even lower footprint: At 183 GHz with the same antenna, the nadir FOV could be on the order of 6 km. Note that the retrieval performances, shown in Section IV, were obtained assuming the different channels to share the same FOV. In case of different FOVs, the results are likely to degrade. An additional analysis considering the spatial correlation of upwelling brightness temperatures and retrieved fields may quantify this degradation, although it is beyond the concept demonstration scope of this paper. The antenna scanning system of FLOMIS remains a major choice to perform: On the one hand, the cross-track LS may ensure a better resolution, a reduced solar intrusion, and a simpler design, but on the other hand, with respect to the CS, it provides a variable polarization and FOV along the scan itself. In order to ensure an accurate Earth pointing (less than 0.1°), each FLORAD platform should be a three-axis-stabilized bus equipped with a stable and precise attitude control subsystem (the orbit control might be neglected, as shown in Fig. 5).

It is worth considering that a non-SS elliptical orbit may require a careful design of the thermal and power subsystem, as the solar incidence angle, with respect to the FC orbital plane, is not constant (the RANN drift may be between 0° and 360° within four months). This might imply that the solar-panel arrays should be movable, or at least canted, to optimize the incident sunlight-power density. The design of the platform structure may be also constrained as more propellant (and bigger tank) is needed, with respect to an equivalent SS-COs, in order to perform the Hohmann transfer maneuvers and to provide a larger platform surface for possible body-mounted solar-panel installations. Finally, the payload-calibration strategy may be also affected due to the variable attitude of each FC platform with respect to the sun as and the satellite eclipses largely vary during one year (from few minutes to 35 min). This aspect constrains the external cold/hot-load-calibration strategy of FLOMIS, designed as a total-power radiometric system (note that the cold load is usually the cosmic background temperature, whereas the hot load is a quasi-optical absorbing reflector).

If properly designed, the FC design can ensure a revisit time of the three-satellite constellation below 2 h, making the FLORAD mission very suitable for atmospheric-nowcasting and civil-protection applications where frequent observation updates are crucial. This revisit time might be even halved (thus becoming comparable to GEO requirements) if the FC could be doubled, i.e., the number of satellites is increased to six by ensuring their orbit phasing [see (3)]. It is worth mentioning that, for a given extension of the target area, the same revisit time is obtained for any equivalent area translated in longitude. This means that the same FC performances, described for the MWM target area, are obtained by choosing the target area of Fig. 1 placed on North America or north Asia between $35^\circ/50^\circ$ latitude. On the other hand, for southern regions corresponding to the perigee, the almost double revisit time is compensated by the increased spatial resolution of radiometer footprint (by a factor of three for FC-ME). Finally, the selected inclination angle equal to $63.4^\circ$ (needed for maintaining a constant apogee) is surely a limitation which prevents the global coverage, typical of a LEO near-polar CO. However, in this respect, the FLORAD mission might be considered complimentary to near-polar LEO missions, similarly to GEO observations which are limited to latitudes of about $\pm 70^\circ$ due to grazing incident angles. All the above features motivate the use of the term "pseudogeostationary scale" adopted to describe the FLORAD small-mission space-time coverage.

## ACKNOWLEDGMENT

The authors would like to thank D. Staelin (MIT, U.S.), C. Accadia (EUMETSAT, D), P. Bauer (ECMWF, U.K.), S. Boukabara (NOAA, U.S.), S. English (MetOffice, U.K.), P. Gaudenzi (Sapienza, I), G. Palmerini (Sapienza, I), A. Hou (NASA, U.S.), S. Leroy (MIT, U.S.), V. Levizzani (CNR, I), J. Junkins (Texas A&M, U.S.), and T. Wilheit (Texas A&M, U.S.) for their helpful discussions and suggestions. They would also like to thank R. Ferretti and E. Pichelli (CETEMPS, I) for providing the MM5 simulations. They would also like to thank the ECMWF staff for atmospheric data set provision.

## REFERENCES

[1] S. Q. Kidder, M. D. Goldberg, R. M. Zehr, M. De Maria, J. F. W. Purdom, C. Velden, N. C. Grody, and S. J. Kusselson, "Satellite analysis of tropical cyclones using the advanced microwave sounding unit," *Bull. Amer. Meteorol. Soc.*, vol. 81, no. 6, pp. 1241–1259, Jun. 2000.

[2] P. Bauer and A. Mugnai, "Precipitation profile retrieval using temperature-sounding microwave observations," *J. Geophys. Res.*, vol. 108, no. D23, pp. 4730–4743, Dec. 2003.

[3] F. W. Chen and D. H. Staelin, "AIRS/AMSU/HSB precipitation estimates," *IEEE Trans. Geosci. Remote Sens.*, vol. 41, no. 2, pp. 410–417, Feb. 2003.

[4] S. A. Boukabara, F. Z. Weng, and Q. H. Liu, "Passive microwave remote sensing of extreme weather events using NOAA-18 AMSUA and MHS," *IEEE Trans. Geosci. Remote Sens.*, vol. 45, no. 7, pp. 2228–2246, Jul. 2007.

[5] D. H. Staelin and C. Surussavadee, "Precipitation retrieval accuracies for geo-microwave sounders," *IEEE Trans. Geosci. Remote Sens.*, vol. 45, no. 10, pp. 3150–3159, Oct. 2007.

[6] D. Cimini, E. R. Westwater, A. J. Gasiewski, M. Klein, V. Ye Leuski, and J. C. Liljegren, "Ground-based millimeter- and submillimeter-wave observations of low vapor and liquid water contents," *IEEE Trans. Geosci. Remote Sens.*, vol. 45, no. 7, pp. 2169–2180, Jul. 2007.

[7] A. J. Gasiewski and D. H. Staelin, "Numerical modeling of passive microwave $O_2$ observations over precipitation," *Radio Sci.*, vol. 25, no. 3, pp. 217–235, May/Jun. 1990.

[8] P. Bauer and S. Di Michele, *Mission Requirements for a Post-EPS Microwave Radiometer*, 2007. Post-EPS EUMETSAT Contract No. EUM/CO/06/1510/PS.

[9] C. Surussavadee and D. H. Staelin, "Global millimeter-wave precipitation retrievals trained with a cloud-resolving numerical weather-prediction model. Part I: Retrieval design," *IEEE Trans. Geosci. Remote Sens.*, vol. 46, no. 1, pp. 109–118, Jan. 2008.

[10] N. Bormann, G. Kelly, P. Bauer, and W. Bell, "Assimilation and monitoring of SSMIS, AMSR-E and TMI data at ECMWF," in *Proc. 15th Int. TOVS Study Conf.*, Maratea, Italy, Oct. 2006.

[11] C. Faccani, D. Cimini, F. S. Marzano, and R. Ferretti, "Three-dimensional variational assimilation of Special Sensor Microwave/Imager data into a mesoscale weather-prediction model: A case study," *Q. J. R. Meteorol. Soc.*, vol. 133, no. 626A, pp. 1295–1307, 2007.

[12] C. A. Mears, M. Schabel, and F. J. Wentz, "A reanalysis of the MSU channel 2 tropospheric temperature record," *J. Clim.*, vol. 16, no. 22, pp. 3650–3664, Nov. 2003.

[13] P. Basili, S. Bonafoni, P. Ciotti, F. S. Marzano, G. d'Auria, and N. Pierdicca, "Retrieving atmospheric temperature profiles from microwave radiometers using a priori information on spatial-temporal correlation," *IEEE Trans. Geosci. Remote Sens.*, vol. 39, no. 9, pp. 1896–1905, Sep. 2001.

[14] P. W. Rosenkranz, "Retrieval of temperature and moisture profiles from AMSU-A and AMSU-B measurements," *IEEE Trans. Geosci. Remote Sens.*, vol. 39, no. 11, pp. 2429–2435, Nov. 2001.

[15] J. Susskind, D. C. Barnet, and J. M. Blaisdell, "Retrieval of atmospheric and surface parameters from AIRS/AMSU/HSB data in the presence of clouds," *IEEE Trans. Geosci. Remote Sens.*, vol. 41, no. 2, pp. 390–409, Feb. 2003.

[16] F. S. Marzano, M. Palmacci, G. Giuliani, D. Cimini, and J. Turk, "Multivariate statistical integration of satellite infrared and microwave radiometric measurements for rainfall retrieval at the geostationary scale," *IEEE Trans. Geosci. Remote Sens.*, vol. 42, no. 4, pp. 1018–1032, May 2004.

[17] F. Romano, D. Cimini, R. Rizzi, and V. Cuomo, "Multilayered cloud parameters retrievals from combined infrared and microwave satellite observations," *J. Geophys. Res.*, vol. 112, p. D08 210, 2007. DOI: 10.1029/2006JD007745.

[18] A. Mugnai, S. Di Michele, E. A. Smith, F. Baordo, P. Bauer, B. Bizzarri, P. Joe, C. Kidd, F. S. Marzano, A. Tassa, J. Testud, and G. J. Tripoli, "Snowfall measurements by proposed European GPM mission," in *Measuring Precipitation From Space—EURAINSAT and the Future*, V. Levizzani, P. Bauer, and F. J. Turk, Eds. New York: Springer-Verlag, 2007, pp. 655–674.

[19] C. Surussavadee and D. H. Staelin, "Global millimeter-wave precipitation retrievals trained with a cloud-resolving numerical weather-prediction model, Part II: Performance evaluation," *IEEE Trans. Geosci. Remote Sens.*, vol. 46, no. 1, pp. 109–118, Jan. 2008.

[20] F. S. Marzano, G. Rivolta, E. Coppola, B. Tomassetti, and M. Verdecchia, "Rainfall nowcast from multisatellite passive-sensor images using recurrent neural network," *IEEE Trans. Geosci. Remote Sens.*, vol. 45, no. 11, pp. 3800–3812, Nov. 2007.

[21] F. J. Tapiador, C. Kidd, V. Levizzani, and F. S. Marzano, "A neural networks-based PMW-IR fusion technique to derive half hourly rainfall estimates at $0.1^\circ$ resolution," *J. Appl. Meteorol.*, vol. 43, pp. 576–594, 2004.

[22] S. Q. Kidder and T. H. Vonder Haar, *Satellite Meteorology. An Introduction*. San Diego, CA: Academic, 1995.

[23] P. Schlüssel, P. Phillips, C. Accadia, R. Munro, S. Banfi, J. Wilson, and L. Sarlo, *Post-EPS Mission Requirements Document*, Jan. 31, 2008. EUMETSAT Document No. EUM/PEPS/REQ/06/0043, Issue v1M Draft.

[24] E. A. Smith, G. Asrar, Y. Furuhama, A. Ginati, A. Mugnai, K. Nakamura, R. F. Adler, M.-D. Cho, M. Desbois, J. F. Durning, J. K. Entin, F. Einaudi, R. R. Ferraro, R. Guzzi, P. R. Houser, P. H. Hwang, T. Iguchi, P. Joe, R. Kakar, J. A. Kaye, M. Kojima, C. Kummerow, K.-S. Kuo, D. P. Lettenmaier, V. Levizanni, N. Lu, A. V. Mehta, C. Morales, P. Morel, T. Nakazawa, S. P. Neeck, K. Okamoto, R. Oki, G. Raju, J. M. Sheperd, J. Simpson, B.-J. Sohn, E. F. Stocker, W. K. Tao, J. Testud, G. J. Tripoli, E. F. Wood, S. Yang, and W. Zhang, *International Global Precipitation Measurement (GPM) Program and Mission: An Overview*, V. Levizzani, P. Bauer, and F. J. Turk, Eds. New York: Springer-Verlag, 2007, pp. 611–653.

[25] W. J. Larson and J. R. Wertz, *Space Mission Analysis and Design*, 3rd ed. Boston, MA: Kluwer, 1999.

[26] S. Q. Kidder and T. H. Vonder Haar, "On the use of satellites in Molniya orbits for meteorological observations of middle and high latitudes," *J. Atmos. Ocean. Technol.*, vol. 7, pp. 517–522, Jun. 1990.
[27] D. Mortari, M. P. Wilkins, and C. Bruccoleri, "The flower constellations," *J. Astronaut. Sci.*, vol. 52, no. 1/2, pp. 107–127, Jan.–Jun. 2004.
[28] O. Abdelkhalik, D. Mortari, and K. J. Park, "Satellite constellation design for earth observation," presented at the 15th AAS/AIAA Space Flight Mechanics Meeting, Copper Mountain, CO, Jan. 23–27, 2005, Paper AAS 05-148.
[29] F. S. Marzano, D. Cimini, M. Montopoli, A. Memmo, R. Ferretti, T. Rossi, M. De Sanctis, M. Lucente, D. Mortari, D. Oricchio, S. Varchetta, P. Pavia, A. Nassisi, M. Balduccini, A. Scorzolini, L. Reboa, P. Tozzi, A. Bruno, F. Greco, G. Perrotta, G. Giuliani, R. Giusto, and S. Di Michele, "FLORAD: Micro-satellite flower constellation of millimeter-wave radiometers for atmospheric remote sensing," in *Proc. MicroRad*, Florence, Italy, Apr. 11–14, 2008, pp. 1–4.
[30] C. Bruccoleri and D. Mortari, "The flower constellations visualization and analysis tool," in *Proc. IEEE Aerosp. Conf.*, Big Sky, MT, Mar. 5–12, 2005, pp. 601–606.
[31] C. D. Rodgers, "Retrieval of atmospheric temperature and composition from remote measurements of thermal radiation," *Rev. Geophys. Space Phys.*, vol. 14, no. 4, pp. 609–624, Nov. 1976.
[32] B. Lambrigtsen and R. Calheiros, "The humidity sounder for Brazil," *IEEE Trans. Geosci. Remote Sens.*, vol. 41, no. 2, pp. 352–361, Feb. 2003.
[33] L. Costesa, C. Bushellb, M. Buckleyb, and G. Masonc, "Microwave humidity sounder (MHS) antenna," in *Proc. SPIE Conf. Sensors, Syst., Next-Generation Satell.*, Florence, Italy, 1999, vol. 3870, p. 412.
[34] A. Stoffelen, M. Bonavita, J. Eyre, M. Goldberg, H. Järvinen, C. Serio, J.-N. Thépaut, and V. Wulfmeyer, *AEG-AS Position Paper—Post-EPS Developments on Atmospheric Sounding and Wind Profiling*, 2006. EUMETSAT Post-EPS Program, Version 2.D 6/03/06.
[35] R. Rizzi, P. Bauer, S. Crewell, M. Leroy, C. Mätzler, W. P. Menzel, B. Ritter, J. E. Russell, and A. Thoss, "AEG-CPL position paper—cloud, precipitation and large scale land," *Surface Imaging (CPL) Observational Requirements for Meteorology, Hydrology and Climate*, 2006. EUMETSAT Post-EPS program, Version 1.k 06/03/06.
[36] S. S. Leroy, J. G. Anderson, and G. Ohring, "Climate signal detection times and constraints on climate benchmark accuracy requirements," *J. Clim.*, vol. 21, no. 4, pp. 841–846, Feb. 2008.
[37] M. De Sanctis, T. Rossi, M. Lucente, M. Ruggieri, D. Mortari, and D. Izzo, "Flower constellation of orbiters for Martian communication," in *Proc. IEEE Aerosp. Conf.*, 2007, pp. 1–11.
[38] F. Caltagirone, P. Spera, R. Vigliotti, and G. Manoni, "SkyMed-COSMO mission overview," in *Proc. IEEE IGARSS*, Seattle, WA, 1998, vol. 2, pp. 683–685.
[39] J. G. Walker, "Satellite constellations," *Brit. Interplanet. Soc.—Journal (Space Technology)*, vol. 37, pp. 559–572, Dec. 1984.
[40] S. Di Michele and P. Bauer, "Passive microwave radiometer channel selection based on precipitation information content estimation," *Q. J. R. Meteorol. Soc.*, vol. 132, no. 617, pp. 1299–1323, 2006.
[41] C. D. Rodgers, "Information content and optimization of high-spectral-resolution measurements," in *Proc. SPIE Opt. Spectroscopic Tech. Instrum. Atmos. Space Res. II*, P. B. Hays and J. Wang, Eds, 1996, vol. 2830, pp. 136–147.
[42] F. Chevallier, S. Di Michele, and A. P. McNally, *Diverse Profile Datasets From the ECMWF 91-Level Short-Range Forecast*, 2006. EUMETSAT NWP SAF Tech. Rep. NWPSAF-EC-TR-010.
[43] P. Bauer, E. Moreau, F. Chevallier, and U. O'Keefe, "Multiple-scattering microwave radiative transfer for data assimilation applications," *Q. J. R. Meteorol. Soc.*, vol. 132, no. 617, pp. 1259–1281, Apr. 2006.
[44] F. S. Marzano, "Modeling antenna noise temperature due to rain clouds at microwave and millimeter-wave frequencies," *IEEE Trans. Antennas Propag.*, vol. 54, no. 4, pp. 1305–1317, Apr. 2006.
[45] J. Dudhia, "A nonhydrostatic version for the Penn-State-NCAR mesoscale model: Validation test and simulation of an Atlantic cyclone and cold front," *Mon. Weather Rev.*, vol. 121, no. 5, pp. 1493–1513, 1993.
[46] T. R. Sreerekha, A. M. Doherty, S. J. English, and P. J. Rayer, *Final Report on The Potential of Microwave Sounder 229 GHz Channel*, Apr. 22, 2008. EUMETSAT Contract EUM/CO/07/4600000409/CJA.
[47] S. English and T. J. Hewison, "A fast generic millimetre wave emissivity model," in *Proc. SPIE Microw. Remote Sensing Atmos. Environ.*, 1998, pp. 22–30.
[48] T. J. Hewison, "Airborne measurements of forest and agricultural land surface emissivity at millimeter wavelengths," *IEEE Trans. Geosci. Remote Sens.*, vol. 39, no. 2, pp. 393–400, Feb. 2001.

**Frank Silvio Marzano** (S'89–M'99–SM'03) received the Laurea degree (*cum laude*) in electrical engineering and the Ph.D. degree in applied electromagnetics from the University of Rome "La Sapienza," Rome, Italy, in 1988 and 1993, respectively.

In 1993, he was with the Institute of Atmospheric Physics, Italian National Council of Research, Rome. From 1994 to 1996, he was a Postdoctorate Researcher with the Italian Space Agency, Rome. In 1997, he was a Lecturer with the University of Perugia, Perugia, Italy. He was with the Department of Electrical Engineering, University of L'Aquila, L'Aquila, Italy, where he cofounded the Center of Excellence CETEMPS. Since 2005, he has been with the Department of Electronic Engineering, University of Rome "La Sapienza," where he is currently teaching courses on antennas and remote sensing. Since 2007, he has also been the Vice Director of the Center of Excellence CETEMPS, University of L'Aquila. His current research concerns passive and active remote sensing of the atmosphere from ground-based, airborne, and spaceborne platforms and radiopropagation topics along satellite microwave links. He has published more than 80 peer-reviewed papers and more than 160 extended abstracts.

Dr. Marzano is a member of the Italian Society of Electromagnetics. He was the recipient of the Young Scientist Award of the XXIV International Union of Radio Science General Assembly in 1993. In 1998, he was the recipient of the Alan Berman Publication Award from the Naval Research Laboratory, Washington, DC. From 2001 to 2005, he was the Italian national delegate for the European COST actions 720 and 280, while since 2008, he has been the Italian delegate for COST IC0802 and ES0702. Since January 2004, he has been acting as an Associated Editor of the IEEE GEOSCIENCE REMOTE SENSING LETTERS. In 2004 and 2006, he was the Coguest Editor of the Special Issues on MicroRad for IEEE TRANSACTIONS ON GEOSCIENCE AND REMOTE SENSING.

**Domenico Cimini** (M'03) was born in Teramo, Italy, in 1973. He received the M.S. (*cum laude*) and Ph.D. degrees in physics from the University of L'Aquila, L'Aquila, Italy, in 1998 and 2002, respectively.

From 1999 to 2001, he has been with the Environmental Technology Laboratory, National Oceanic and Atmospheric Administration (NOAA), Boulder, CO. From 2002 to 2004, he was with the Center of Excellence for Remote Sensing and Modeling for the Forecast of Severe Weather (CETEMPS), University of L'Aquila. From 2004 to 2005, he was a Visiting Fellow in the Cooperative Institute for Research in Environmental Sciences, University of Colorado, Boulder. From 2005 to 2006, he was with the Institute of Methodologies for the Environmental Analysis, Italian National Research Council, where he worked on ground- and satellite-based observations of cloud properties. Since 2006, he has been with the Center for Environmental Technology, Department of Electrical and Computer Engineering, University of Colorado, where in 2007, he was an Adjunct Professor. He is currently a Research Assistant with the Center of Excellence CETEMPS, University of L'Aquila. He coauthored more than 20 peer-reviewed papers and more than 50 extended abstracts.

Dr. Cimini was the recipient of the Fondazione Ugo Bordoni Award 2008 in memory of Prof. Giovanni D'Auria.

**Adelaide Memmo** received the Laurea degree in astronomy from the University of Bologna, Bologna, Italy, in 1996.

Between 1997 and 2002, she was a Researcher with the Scientific and Technological Park, Abruzzo, Italy. Since 2003, she has been a Research Scientist with the Center of Excellence CETEMPS, University of L'Aquila, L'Aquila, Italy, where she is focusing her activity on meteorological modeling, radiative transfer, and microwave radiometry.

**Mario Montopoli** received the Laurea degree in electronic engineering from the University of L'Aquila, L'Aquila, Italy, in 2004 and the Ph.D. degree in radar meteorology from the University of Basilicata, Potenza, Italy, and the University of Rome "La Sapienza," Rome, Italy, in 2008, through a joint program.

Since 2005, he has been with the Center of Excellence CETEMPS, University of L'Aquila, where he is a Research Scientist on ground-based radar meteorology and satellite meteorology. Since 2006, he is also a Research Assistant with the Department of Electrical Engineering and Information.

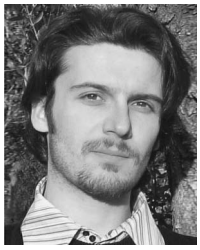

**Tommaso Rossi** received the University degree in telecommunications, the M.Sc. degree in "advanced communications and navigation satellite systems," and the Ph.D. degree in telecommunications and microelectronics from the University of Rome "Tor Vergata," Rome, Italy, in 2002, 2004, and 2008, respectively.

He is currently an Assistant Professor with the Department of Electronic Engineering, University of Rome "Tor Vergata." He is a member of the Italian Space Agency W-band Analysis and VErification (WAVE) Project Technical Team, a feasibility study for W-band telecommunication payloads. He is part of the scientific team that is defining the TDP#5 payload embarked on ESA Alphabus satellite. He has been a Technical Member of the ESA research project on Flowers Constellations. His research activity is focused on space systems, EHF satellite telecommunications, satellite and inertial navigation systems, digital signal processing, and satellite constellations.

**Mauro De Sanctis** received the "Laurea" degree in telecommunications engineering and the Ph.D. degree in telecommunications and microelectronics engineering from the University of Rome "Tor Vergata," Rome, Italy, in 2002 and 2006, respectively.

He was involved in the MAGNET European FP6 integrated project and in the SatNEx European network of excellence. In autumn of 2004, he was with CTIF, University of Aalborg, Aalborg, Denmark, which is a research center focusing on modern telecommunications technologies. In 2006, he was a Postdoctoral Research Fellow for the ESA/ARIADNA extended study on the Flower Constellations. He is involved in several Italian national research projects. He is currently with the Department of Electronic Engineering, University of Rome "Tor Vergata." His main areas of interest are in satellite networks and constellations (in particular, Flower constellations), stratospheric platforms, and resource management of short-range wireless systems.

Dr. De Sanctis is currently an Associate Editor of the IEEE AEROSPACE AND ELECTRONIC SYSTEMS MAGAZINE.

**Marco Lucente** received the University degree in physics with specialization of astrophysics and space physics from the University of Rome "La Sapienza," Rome, Italy, in 2002 and the M.Sc. degree in "advanced communication and navigation satellite systems" from the University of Rome "Tor Vergata," Rome, in 2005.

Since the beginning of 2004, he has been working as a Scientific Member of the W-band Analysis and VErification (WAVE) Project Team. He was involved in studying the polarimeter of the Balloon Observation of Millimetric Extragalactic Radiation and Geophysics (BOOMERanG) experiment. He is currently with the Department of Electronic Engineering, University of Rome "Tor Vergata." His main fields of research concern space systems, EHF telecommunication satellites, scientific satellites, navigation satellite systems, inertial navigation systems, and lunar and martian communication and navigation systems.

**Daniele Mortari** (M'03) received the Laurea degree on nuclear engineering from the University of Rome "La Sapienza," Rome, Italy, in 1981.

He is currently an Associate Professor with the Department of Aerospace Engineering, Texas A&M University, College Station. He is active in the fields of orbital mechanics, attitude determination, star navigation, data processing, and matrix analysis. He is the author of more than 120 papers.

Dr. Mortari was the recipient of the NASA Award for the San Marco V Mission, the Spacecraft Technology Center Award for the StarNav I Experiment on the STS-101, and the 2007 IEEE Judith A. Resnik Award. He is member of the AAS Space Flight Mechanics Technical Committee. He is the Associate Editor of *Journal of the Astronautical Sciences*, of the *Transactions on Aerospace and Electronic Systems*, and of the *International Journal of Navigation and Observations*.

**Sabatino Di Michele** received the Laurea degree in electronic engineering and the Ph.D. degree in information and electrical engineering from the University of L'Aquila, L'Aquila, Italy, in 1997 and 2004, respectively.

Since the beginning of 1998, he has been collaborating with the Department of Electrical Engineering, University of L'Aquila, where he has been working on SSM/I applications and ground-based radiometry. In November 1998, he was with the Institute of Atmospheric Physics, Italian National Council of Research, Rome, Italy, where he worked on rainfall retrieval techniques for the Tropical Rainfall Measuring Mission (TRMM) microwave instruments. He is currently with the European Centre for Medium-range Weather Forecast (ECMWF), Reading, U.K., where he is working on issues related to rainfall assimilation. He has been participating in various international projects (e.g., EuroTRMM, Eurainsat). He is also involved in the research activity of the planned Global Precipitation Measurement Mission. His studies are mainly focused on radiative-transfer modeling and on the development of new inversion procedures.